The Hemodynamic Basis for Positional- and Inter-Fetal Dependent Effects in Dual Arterial Supply of Mouse Pregnancies

Tal Raz[1][9], Reut Avni[1][9], Yoseph Addadi[1], Yoni Cohen[1], Ariel J. Jaffa[2], Brian Hemmings[3], Joel R. Garbow[4], Michal Neeman[1]*

1 Department of Biological Regulation, Weizmann Institute of Science, Rehovot, Israel, 2 Lis Maternity Hospital, Tel Aviv Souraski Medical Center, Tel Aviv, Israel, 3 Friedrich Miescher Institute for Biomedical Research, Basel, Switzerland, 4 Biomedical MR Laboratory, Mallinckrodt Institute of Radiology, Washington University, St. Louis, Missouri, United States of America

Abstract

In mammalian pregnancy, maternal cardiovascular adaptations must match the requirements of the growing fetus(es), and respond to physiologic and pathologic conditions. Such adaptations are particularly demanding for mammals bearing large-litter pregnancies, with their inherent conflict between the interests of each individual fetus and the welfare of the entire progeny. The mouse is the most common animal model used to study development and genetics, as well as pregnancy-related diseases. Previous studies suggested that in mice, maternal blood flow to the placentas occurs via a single arterial uterine loop generated by arterial-arterial anastomosis of the uterine artery to the uterine branch of the ovarian artery, resulting in counter bi-directional blood flow. However, we provide here experimental evidence that each placenta is actually supplied by two distinct arterial inputs stemming from the uterine artery and from the uterine branch of the ovarian artery, with position-dependent contribution of flow from each source. Moreover, we report significant positional- and inter-fetal dependent alteration of placental perfusion, which were detected by in vivo MRI and fluorescence imaging. Maternal blood flow to the placentas was dependent on litter size and was attenuated for placentas located centrally along the uterine horn. Distinctive apposing, inter-fetal hemodynamic effects of either reduced or elevated maternal blood flow, were measured for placenta of normal fetuses that are positioned adjacent to either pathological, or to hypovascular *Akt1*-deficient placentas, respectively. The results reported here underscore the critical importance of confounding local and systemic in utero effects on phenotype presentation, in general and in the setting of genetically modified mice. The unique robustness and plasticity of the uterine vasculature architecture, as reported in this study, can explain the ability to accommodate varying litter sizes, sustain large-litter pregnancies and overcome pathologic challenges. Remarkably, the dual arterial supply is evolutionary conserved in mammals bearing a single offspring, including primates.

Introduction

Pregnancy in mammals requires coordinated adaptation of the systemic maternal cardiovascular system and remodeling of the entire uterine circulation, to assure adequate oxygenation and nutrient delivery to the developing embryo/fetus [1–3]. A variety of prenatal syndromes in humans, including intrauterine growth restriction (IUGR), preeclampsia, and fetal death in utero have been attributed to insufficient placental perfusion. Maternal vascular adaptation to pregnancy includes vascular remodeling, increased uterine blood flow, and systemic increase in total blood volume and cardiac output [1,4–8]. The consequences of placental malfunction include predisposition to systemic cardiovascular and pulmonary vascular dysfunction [9–12] associated with increased risk for ischaemic heart disease throughout life [13,14].

To insure successful reproduction, mammals have adopted one of two primary strategies. In some species, including humans, non-human primates and horses, single-fetus pregnancy was optimized for high survival rate. The alternative strategy, found for example in porcine, canines, felines and rodents, is delivery of large litters. To achieve large successful litters, the reproductive system must be optimized in the face of an inherent conflict between the benefit to each individual fetus and the benefit to the species. An important example of large-litter pregnancy is the mouse. The uterus of the mouse is duplex, composed of two independent uterine horns that converge at the cervix [15]. Blood enters the mouse uterus cranially through the uterine branch of the ovarian artery and caudally through the uterine artery [15,16]. Studies of McLaren and Michie in the late 1950s reported that pregnancy is supported in each of the two uterine horns by a single uterine arterial loop,

which is generated by direct artery-to-artery anastomosis of the uterine artery with the uterine branch of the ovarian artery [15–17]. The direction of blood flow in the single uterine arterial loop was described as being dominated by the uterine branch of the ovarian artery in the cranial portion of each horn, and by the distal part of the uterine artery on the caudal end. Such counter flow within this single loop was postulated to result in a significant drop in pressure and flow velocity to the central embryos/fetuses in each uterine horn [16,17]. We argue that such an anatomical structure, including opposing flow within a single arterial loop, results in a hemodynamic enigma, in which the central fetuses receive little or even zero perfusion. This appears to be an unfavorable structure for maintaining stable and robust distribution of perfusion between placentas in a large litter, as the middle fetuses may not survive the course pregnancy. Moreover, opposing flow within a single arterial loop is unreasonable in terms of the hemodynamics of blood flow.

To evaluate the anatomy and function of maternal circulation to support pregnancy in the mouse, we adopted state-of-the-art, non-invasive imaging tools. Over the last years, there has been significant progress in non-invasive imaging of mouse pregnancy [18–24]. These studies have focused on imaging anatomical details in developing embryos [25,26] by ultrasound and MRI [22], and, in particular, analysis of the fetal heart and brain [27–30]. In addition, using ferritin as a reporter gene for MRI, we reported in vivo identification of fetal vascular development through the expression of VE-cadherin [31]. Furthermore, a number of studies investigated perfusion of the placenta in mice using contrast media such as GdDTPA and biotin-BSA-GdDTPA [19,24,32]. Of particular interest was the use of MRI for analysis of fetal development in Akt1-deficient mice. Akt1, also known as PKB alpha, is a major component of growth-factor-induced signaling, and was found to play a critical role in angiogenesis, cell survival and differentiation, and glucose metabolism [33]. Akt1 deficiency leads to in utero growth retardation and death associated with deficiencies in placental vascularity [18,34–37]; therefore, Akt1 deficient mice have been suggested as a model for human IUGR [18,38].

One of the complications of longitudinal studies of mouse pregnancy is the accurate identification of embryos in utero. We recently introduced the use of bi-directional arterial spin labeling MRI (BD-ASL MRI) for identification of fetal order along the uterus horn in vivo, based upon the specific pattern of the dual arterial blood supply within the mouse uterine horns [39]. Peak BD-ASL values showed highly significant positive correlation to the position of placentas along the uterine horn: peak BD-ASL values were found to be negative for placentas near the cervix and increased gradually for the middle placentas, with the placenta closest to the ovary having the largest positive signal. This ability to non-invasively determine fetus location along the uterine horn opened possibilities for determining and pursuing phenotypic alterations in genetic, as well as developmental, longitudinal studies.

The aim of the current study was to examine the hemodynamics of maternal circulation in mice, and to evaluate how it balances between the needs of individual fetuses and the entire litter to guarantee successful pregnancy. The anatomical description, and particularly the concept of bidirectional flow within a single uterine arterial loop, was revisited, using state-of-the-art imaging methods. We further analyzed the patterns of maternal-to-fetal water exchange and maternal blood volume in placentas during normal pregnancy, as well as in pregnancies complicated by spontaneous missed abortions, surgical ligation of specific arterial

input, and genetic in utero growth retardation due to thymoma viral proto-oncogene 1 (Akt1) deficiency [18,34–36].

Materials and Methods

Animal Models

All experiments were approved by the Institutional Animal Care and Use Committee (IACUC) of the Weizmann Institute of Science (Permit Number: 03020610-2). Female ICR mice (n = 11 dams, 86 placentas/fetuses) and B6(C57BL/6J)/$Akt1^{+/-}$ mice (n = 17 dams, 128 fetuses/placentas) were analyzed on embryonic day E17.5 (E0.5 = day of vaginal plug, which indicates mating). Multimodal imaging consisted of: 1) in vivo, whole body, non-invasive MR imaging, including fast spin-echo MRI followed by BD-ASL MRI [39], 2) in vivo intravital microscopy of surgically-exposed uterine horns following intravenous administration of fluorescent FITC-dextran, and 3) ex vivo FITC-dextran fluorescence analysis of the maternal blood volume in the same placentas (Fig. 1).
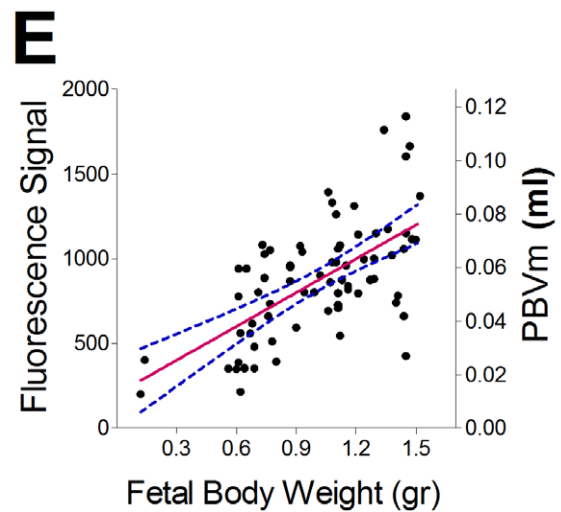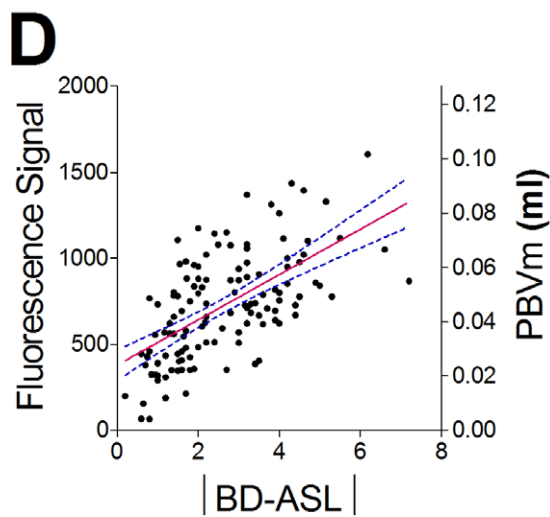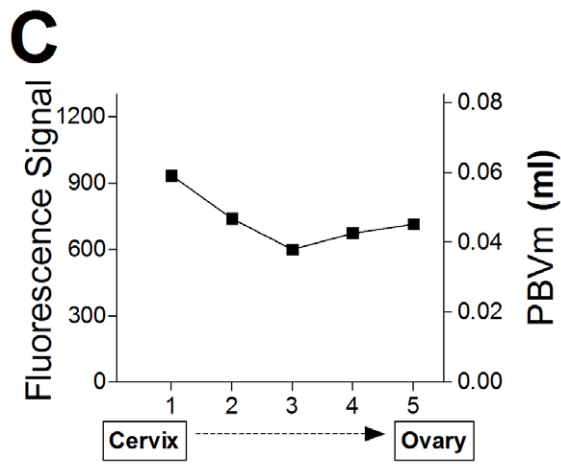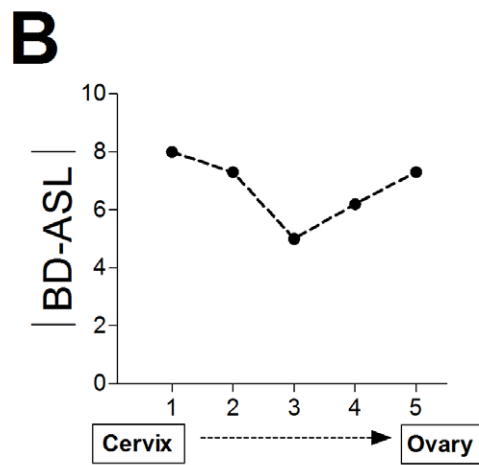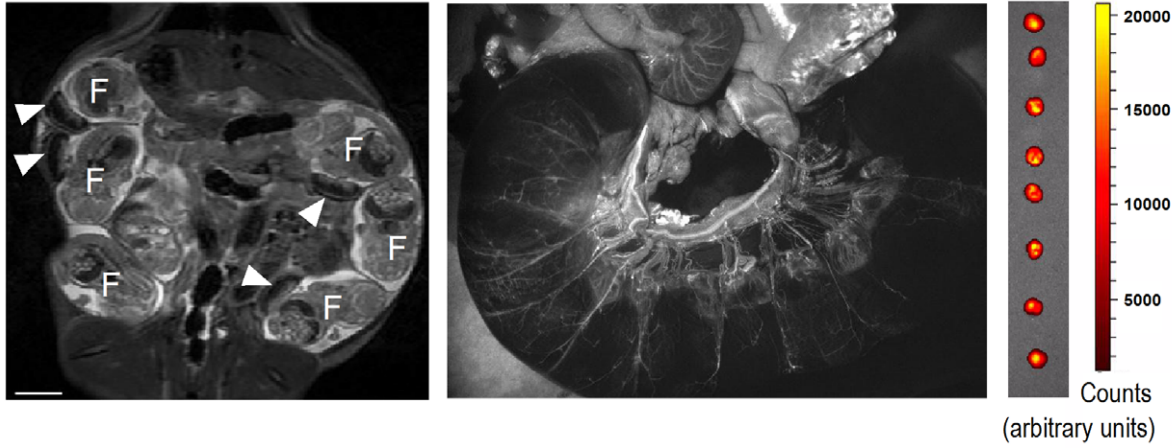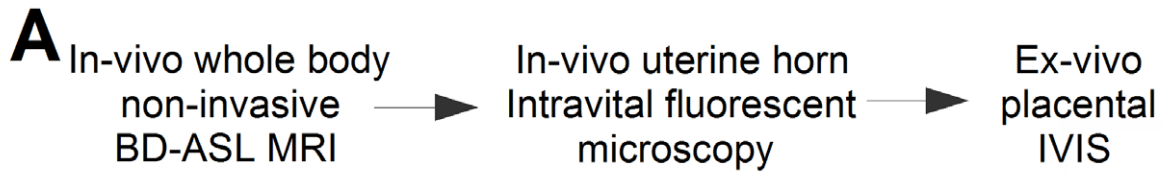
In Vivo MRI Studies

MRI experiments were performed at 9.4T on a BioSpec 94/20 USR spectrometer (Bruker; Karlsruhe, Germany). A quadrature volume coil (72 mm i.d.) was used for both transmit and receive. Anesthetized mice (isoflurane, 3% for induction, 1–2% for maintenance; Abbott Laboratories Ltd, England; in oxygen,1 liter/min delivered through a muzzle mask) were placed in a supine position, with respiratory and thermal monitoring (SA Instruments Model 1025 monitoring and gating system, Stony Brook, NY, USA; 50–70 breaths per min; 37°C body temperature, maintained using a circulating water system).

Fast spin-echo MRI using a RARE sequence (Rapid Acquisition with Refocused Echoes) was used to visualize all feto-placental units using the following parameters: effective echo time (TE) = 85.5 ms; RARE factor = 8; slice thickness 1.0 mm; inter-section gap 0.2 mm; matrix 256×128, zero filled to 256×256; coronal: repetition time (TR) = 3000 ms; field of view (FOV) = 7×5 cm²; axial: TR = 4000 ms; FOV = 5×5 cm²; 15–40 slices were acquired to cover all the feto-placental units.

Placental perfusion was measured using Bi-Directional Arterial Spin Labeling data (BD-ASL), as described by Avni, et al. [39]. Briefly, multi-slice, axial two-dimensional gradient echo (2D–GE) data were acquired with the following parameters: TR = 53 ms; TE = 3.2 ms; slice thickness = 1.0 mm; intersection gap 0.2 mm; 4 slices per scan; FOV = 5×5 cm²; matrix = 256×128, zero filled to 256×256; 10 dummy scans; 32 averages; and a scan time with respiratory gating ~6 min). A thick axial slice (8 mm) was used for saturation of blood in either the maternal heart or the bifurcation point of the common iliac artery (90° hermit pulse, 2 ms followed by a crusher gradient). BD-ASL data were analyzed with in-house programs written in Matlab (Mathworks; Natick, MA, USA), using the normalized percentile difference between the two acquired images:

$$BDASL = \left(\frac{SI_{lower}}{\max(SI_{lower})} - \frac{SI_{upper}}{\max(SI_{upper})} \right) \times 100$$

where SI_{upper} and SI_{lower} are the magnetization in the perfused organ with upper and lower steady-state saturation pulses, respectively [39]. The resulting analyses were used to produce saturation transfer BD-ASL maps, in which a change in signal intensities revealed the directional contribution of water exchange between the maternal blood and the placenta; accordingly, the signal in each placenta was color-coded (as blue or red pixels)

A In-vivo whole body non-invasive BD-ASL MRI → In-vivo uterine horn Intravital fluorescent microscopy → Ex-vivo placental IVIS

Counts (arbitrary units)

Figure 1. Position dependence of maternal blood to placentas along the uterine horn. (A) Experimental scheme for multi-modal functional imaging of pregnant mice: pregnant female ICR mice (E17.5) were analyzed using MRI, intravital fluorescence microscopy, and ex vivo fluorescence analysis of the maternal blood volume in the placenta (PBVm). Note fetuses (F) and their placentas (white arrow heads). (B) Data for a pregnant mouse carrying 5 fetuses in one uterine horn. Position dependence of maternal bi-directional perfusion was detected by MRI (|BD-ASL|). (C) Ex vivo fluorescence and corresponding PBVm values for the placentas in one uterine horn, in the same pregnant mouse as in A. (D) Correlation between PBVm and |BD-ASL| (n = 11 dams, 86 placentas/fetuses; r = 0.62, $P < 0.0001$). (E) Correlation between PBVm and fetal body weight (n = 11 dams, 86 placentas/fetuses; r = 0.64, $P < 0.0001$).
doi:10.1371/journal.pone.0052273.g001

according to its blood origin (i.e., uterine artery, or uterine branch of the ovarian artery, respectively). Placenta BD-ASL values depend on the contribution of the arterial supply direction: negative values represent placentas that are perfused more dominantly by the uterine artery, and positive values represent placentas that are nourished more dominantly by the uterine branch of the ovarian artery [39]. The absolute value of BD-ASL is proportional to tissue perfusion, namely the exchange of water across the labyrinth within the placenta.

Fluorescence Analysis of the Uterine Blood Supply

The uterine blood supply was imaged using a Zoom Stereo Microscope SZX-RFL-2 (Olympus, Tokyo, Japan) equipped with a fluorescence illuminator and a Pixelfly camera (PCO, Kelheim Germany), and analyzed using ImageJ (http://rsbweb.nih.gov/ij/). Mice were anesthetized with Ketamin (i.p.; Ketaset®, Fort Dodge Laboratories, Fort Dodge, IA, USA; 100 mg/kg) and Xylazine (i.p.; XYL-M, VMD, Arendonk, Belgium; 16 mg/kg). The uterus was surgically exposed through a ventral midline celiotomy and the two uterine horns were spread out to expose the intact blood vessels. Dextran–fluorescein isothiocyanate (6 mg diluted in 300 µl PBS per animal; FITC, 500 kDa; Sigma Aldrich) was injected via a tail-vein catheter for acquisition of dynamic data (1200 frames/min for 0.5 min; exposure time of 50 ms; excitation 460 – 490 nm; emission 510 – 550 nm). Preliminary experiments revealed an equilibration time of 10 minutes in order to reach a steady-state fluorescent signal in the placental vasculature. Thus, the reported fluorescent intensity was acquired 10 minutes after administration of the contrast media. Signal enhancement was normalized for each placenta, using the pre-injection value.

Ex vivo fluorescence studies of maternal blood volume in the placentas were performed using an IVIS 100 Imaging System (Xenogen; Cranbury, NJ, USA; excitation 500 nm; emission 540 nm). Placental fluorescence was normalized to the intra-vital signal measured in the uterine artery 10 minutes post FITC-dextran administration.

Placental maternal blood volume (PBVm; in ml) was derived using calibration measurements on blood samples from ICR female mice 10 min after intravenous dextran-FITC administration (n = 6; E17.5). The fluorescence of blood samples (0.01, 0.03, 0.05, 0.08, 0.1, 0.15, 0.3 ml; IVIS), normalized to the intravital fluorescence in the uterine artery, was positively correlated to the blood volume (r = 0.97, $P < 0.0001$; Fig. S1). Using this calibration, the estimated PBVm in the examined placentas of this group of mice (mean ± SEM) was calculated to be 0.072 ± 0.002 ml.

Ligation of Arterial Blood Supply to the Uterine Horn

Arterial ligations were performed on anesthetized pregnant ICR mice (E17.5, n = 20). The uterus was surgically exposed through a ventral midline celiotomy. Surgical ligations were performed in either the uterine branch of the ovarian artery (n = 10 mice, 5 mice on each side; 82 placentas/fetuses), or in the uterine artery (n = 10 mice, 5 mice on each side; 92 placentas/fetuses), using a Surgeon Knot (PDS 5–0 suture material, Ethicon, San Angelo, TX, USA). Immediately after the ligation, mice were positioned

for fluorescence intravital imaging using dextran-FITC administration, as described above. The fluorescence signal in each placenta in the ligated side was calibrated to the average fluorescence of all placentas in the control side. The relative contribution of each ligated artery to the overall placental blood volume in the horn, in each animal, was calculated according to the following equation:

$$Overall\ relative\ arterial\ contribution(\%) =$$
$$\left[1 - \frac{average(SI_{ligation\cdots side})}{average(SI_{control\cdots side})}\right] \times 100$$

The position-dependent contribution of each artery to each placenta was calculated using the data obtained only from those animals which had a symmetric pregnancy (either 4 fetuses/placentas in each uterine horn, n = 5 dams; or 6 fetuses/placentas in each uterine horn, n = 4 dams), according to the following equation:

$$Relative\ arterial\ contribution\ to\ specific\ placenta(\%) =$$
$$\left[1 - \frac{SI_{(ligation\ side)}}{SI_{(control\ side)\ in\ parallel\ location}}\right] \times 100$$

where SI(ligation or control side) is the fluorescence signal in a placenta located in the same position along the uterine horn in the ligated or control side, respectively.

Validation of Fetal Location and Genotype

For all animals, the positions of the uterus and all fetuses/placentas were recorded by digital camera during ventral midline celiotomy surgery, as described above, or following euthanasia by cervical dislocation. In B6(C57BL/6J)/$AktI^{+/-}$ mice, a sample was taken from the tail of each fetus for genotyping when placentas were obtained for ex vivo fluorescence analysis.

Histology and Fluorescence Microscopy

Placentas were fixed in Carnoy solution, embedded in paraffin, sectioned serially (4 µm thickness), and stained with hematoxylin and eosin (H&E; Sigma-Aldrich) or with 4′,6-diamidino-2-phenylindole (DAPI; Vector Laboratories, Burlingame, CA, USA). Images were obtained with a Zeiss Axio observer microscope (Yena, Germany) equipped with a fluorescence illuminator and an Olympus DP72 camera (Center Valley, PA, USA; FITC, 440 – 470 nm excitation and 525 – 550 nm emission; DAPI, 365 nm excitation and 445 – 450 nm emission).

Statistical Analysis of the Experimental Data

Statistical analyses were performed with analytic computerized software (Statistix 8 Student Edition, Analytical Software, Tallahassee, FL, USA). The general effects of placental location, litter size, and fetal body weights on BD-ASL and fluorescent measurements (intravital microscopy or IVIS data) were analyzed

in a General Analysis of Variance Test (ANOVA), followed by Tukey HSD All-Pairwise Comparisons test. Continuous data were evaluated for normality of distribution and for equality of variances using the Shapiro-Wilk Test and the Bartlett's Test, respectively. Pearson's Correlation Test was used to determine various correlations between BD-ASL, ex vivo placental fluorescence signal, placenta location, litter size, and fetal body weight. Pearson Chi-square Test analysis was used to compare proportional data. Differences were considered significant at $P<0.05$. Unless otherwise noted, results are presented as mean ± SEM.

Modeling the Pattern of Arterial Blood Supply to the Uterine Horns by Electrical Circuit

Maternal circulation in the uterus was modeled as an electrical circuit, with maternal cardiac output simulated by a single, constant voltage (V_H) battery. The current in each placenta was derived numerically using a computer simulation program, PSPICE 9.1 (Cadence, http://www.cadence.com), with simulations based upon standard KCL (Kirchhoff current law) and KVL (Kirchhoff voltage law) analysis.

Results

Maternal Blood Volume and Exchange are Attenuated for Placenta Located Centrally along the Uterine Horn

To evaluate the maternal-to-placental arterial exchange and placental maternal blood volume, a multi-modality imaging approach was applied in ICR pregnant mice on embryonic day E17.5. The multimodal imaging consisted of MRI, intravital microscopy, and fluorescence analysis of the maternal blood volume in the same placentas (PBVm; Fig. 1A–C). Peak BD-ASL values (n = 11 dams; 83 placentas/fetuses) were consistent with fetal position along the uterine horn, as reported previously [39]. Absolute BD-ASL values (|BD-ASL|), corresponding to maternal-fetal arterial water exchange, were significantly larger for the placentas that were positioned at the two extremes of the horns, compared to those in the middle ($P=0.0034$). Furthermore, |BD-ASL| values were significantly larger for placentas adjacent to the cervix, compared to those closer to the ovary ($P=0.0107$).

Within animals, placental fluorescence values and corresponding PBVm displayed a U-shaped pattern, with larger values of enhancements for the placentas located near the origin of blood vessels ($P<0.02$; Fig. 1B, 1C). Overall, PBVm was positively correlated with fetal body weight (Fig. 1E; r = 0.64, $P<0.0001$). |BD-ASL| values (maternal-to-placental arterial exchange) significantly correlated with placental FITC-dextran fluorescence (PBVm; Fig. 1D; r = 0.62, $P<0.0001$).

Effects of Litter Size and the Position along the Uterine Horn on Placental Perfusion

Bi-directional ASL methodology was employed to explore the pattern of transfer of saturated blood to the placentas along the uterine horns in pregnant mice at late gestation. For placentas positioned closer to the cervix, mainly negative BD-ASL contrast voxels were observed (Fig. 2A, blue), consistent with the predominant contribution of maternal blood flow through the uterine artery. In placentas closer to the ovary, the BD-ASL contrast consisted mainly of positive voxels (Fig. 2C), indicating that in the cranial portion of the uterine horn, the major blood supply is through the uterine branch of the ovarian artery. Interestingly, for placentas located in the central region of particularly crowded horns, the BD-ASL contrast inside the placenta included both negative (Fig. 2B, blue) and positive

(Fig. 2B, red) voxels, consistent with a dual supply from both the uterine artery and the uterine branch of the ovarian artery, respectively. Moreover, for all placentas, maternal arterial input was consistent with distinct irrigation fields for each arterial input, while inconsistent with a single mixed arterial input, as would be expected for anastomosis of the two arteries.
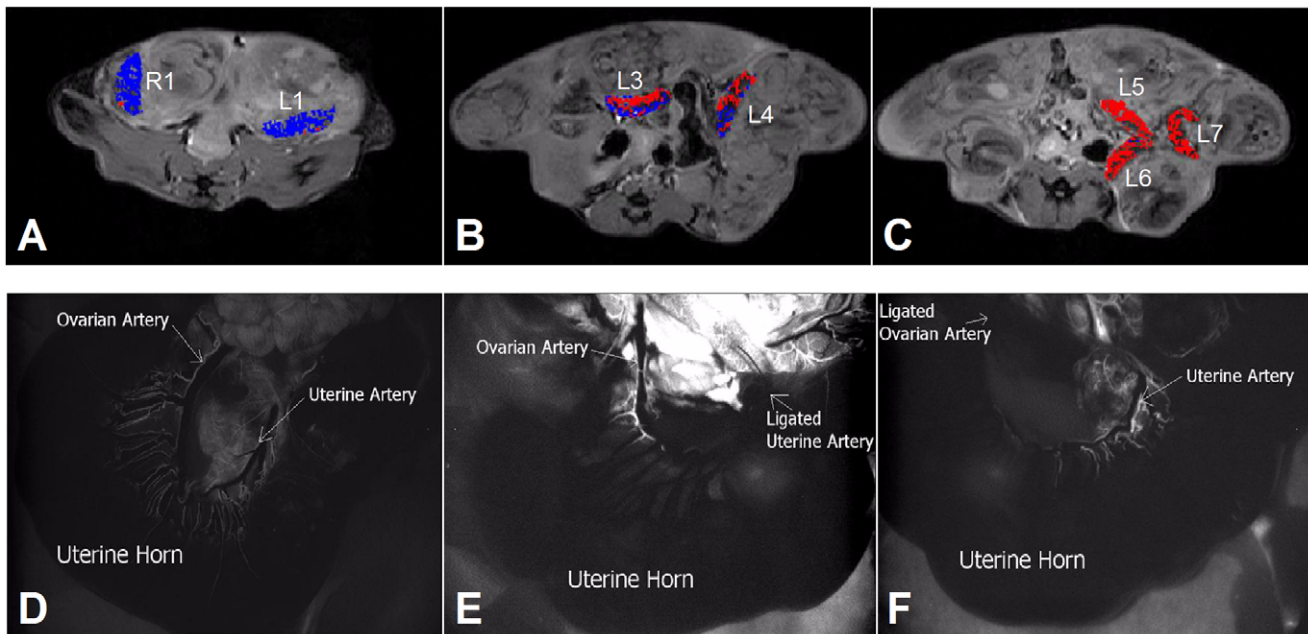
In order to determine the selective contribution of each arterial blood supply to the uterine horn, selective surgical arterial ligations (either the uterine artery, or the uterine branch of the ovarian artery) were performed on anesthetized ICR pregnant mice (E17.5); the exposed intact uterine horns were imaged by fluorescence intravital microscopy following dextran-FITC administration, while the arterial blood vessels to the uterine horns and the placentas were imaged (Fig. 2D–F, represent Movies S1, S2, and S3 for non-ligated control, ligation of the uterine artery, and ligation of the uterine branch of ovarian artery, respectively). Thereafter, the ex vivo fluorescence signals in all placentas were measured, as described in Methods. The type of ligation (uterine artery vs. uterine branch of ovarian artery) had a significant effect on the relative FITC-dextran fluorescence in the corresponding placentas, as well as on the signal dynamics in the major arteries supplying the uterine horn ($P<0.0001$).

Ligation of the uterine artery caused a marked position-dependent reduction in the fluorescence signal in most of the placentas along the uterine horn, as compared to placentas along the non-ligated horn (for specific examples see Fig. 3A and 3B). Ligations of the uterine branch of the ovarian artery resulted in less remarkable changes in the fluorescence-signal intensities of the placentas (for specific examples see Fig. 3C and 3D); the placenta closest to the ligation point (nearest the ovary) displayed only moderate reduction in fluorescence, whereas placentas located near the cervix exhibited almost no reduction in signal. Histological analysis of the placentas demonstrated a decreasing gradient of fluorescent signal enhancements from the ligation points onwards (Fig. 3E and 3F).

The mean ex vivo placental fluorescence intensity in the ligated horn (relative to the mean signal in the non-ligated horn) was significantly affected by the type of ligation, with ligation of the uterine artery causing a larger reduction in signal compared to ligation of the uterine branch of the ovarian artery (Fig. 4A and 4B; $P<0.0001$). The side of the ligation (left vs. right; Fig. 4A) had no effect (uterine ligations: $P=0.758$; uterine branch of ovarian artery: $P=0.43$). The relative contribution of each artery to the fluorescence was calculated for the placentas along the uterine horn (mean [95% CI]). Overall, the uterine artery contributed 68% [55%–82%], while the uterine branch of the ovarian artery contributed 32% [18%–45%]. The contribution of each artery to each placenta was affected by litter size and the location of the placentas along the uterine horn (Fig. 4D and 4E).

Intra-Uterine Neighbor Effect: Sibling Implanted Adjacent to a Pathological/Dead Fetus Exhibits Reduced |BD-ASL| and PBVm

In mice, as in any other litter-bearing mammals, the fetuses must share space in the uterus, suggesting that different fetuses might be exposed to different local environments. Litter size had a systemic effect on fetal body weight (r = −0.7838, $P<0.0001$). Larger litters were associated with higher incidence of severe fetal pathology/death (r = 0.6768, $P<0.0001$). Fetal death/pathology showed no positional dependence along the uterine horn ($P=0.6931$). However, some effects were position dependent (Fig. 5); thus, beyond the expected low |BD-ASL| and PBVm

Figure 2. Assessment of the arterial blood supply to the placenta via BD-ASL MRI and intravital fluorescence microscopy. Two methods were used to explore the pattern of transfer of arterial blood to the placentas along the uterine horns in pregnant mice at late gestation (E17.5): 1) Bi-directional ASL methodology (Panels A–C); and 2) Intravital fluorescence microscopy imaging of the uterine arterial blood supply subsequent to intravenous administration of FITC-dextran to mice having undergone surgical arterial ligations of either the uterine branch of the ovarian artery, or the uterine artery (Panels D–F). (A–C) Placental saturation transfer maps obtained by BD-ASL MRI of an ICR pregnant mouse (E17.5). For placentas positioned closer to the cervix (Panel A: L1, R1), mainly negative BD-ASL contrast voxels (blue) were observed, consistent with the predominant contribution of maternal blood flow through the uterine artery. In placentas closer to the ovary (Panel C: L5–7), the BD-ASL contrast was mainly of positive voxels (red), implying that placentas in this part of the uterine horn are supplied through blood mainly from the uterine branch of the ovarian artery. Placentas located in the central region of the uterine horn (Panel B, L3–4) had a dispersive pattern of BD-ASL values with both negative and positive voxels, consistent with a dual supply from both the uterine artery and the uterine branch of the ovarian artery, respectively. (D) Intravital fluorescence microscopy image of the arterial blood supply to an intact uterine horn (a snapshot from Movie S1). (E) Intravital fluorescence microscopy image of the arterial blood supply to a uterine horn following ligation of the uterine artery (a snapshot from Movie S2). (F) Intravital fluorescence microscopy image of the arterial blood supply to a uterine horn following ligation of the uterine branch of the ovarian artery (a snapshot from Movie S3).
doi:10.1371/journal.pone.0052273.g002

values for placenta of pathological fetuses, the placenta located nearest to the pathological one also exhibited relatively low |BD-ASL| and PBVm values, compared with those predicted based on its location along the uterine horn (Fig. 5A).

To evaluate the impact of spontaneous fetal pathology/death on its neighbouring siblings in utero, all examined placentas (n = 11 mothers; 83 placentas/fetuses) were analyzed (Fig. 5B and 5C). Both |BD-ASL| and PBVm values of the placentas of pathological fetuses (|BD-ASL|: 1.3 ± 0.1; PBVm: 0.030 ± 0.003 ml), as well as their normal adjacent neighbours (|BD-ASL|: 1.7 ± 0.2; PBVm: 0.035 ± 0.004 ml), were significantly lower ($P<0.008$) compared to placentas lacking a neighbouring pathological fetus (|BD-ASL|: 3.0 ± 0.2; PBVm: 0.060 ± 0.002 ml). These results are consistent with a pathological/dead fetus having a significant negative influence on its most adjacent neighbouring sibling(s).

Akt1$^{+/+}$ Sibling Implanted Adjacent to an Akt1$^{-/-}$ Placenta/Fetus Shows Increased |BD-ASL| and PBVm

Thymoma viral proto-oncogene 1 (*Akt1*) plays an important role as an angiogenesis mediator and in placental vascular and cardiac function [18,40]. It was shown previously that *Akt1*$^{-/-}$ placentas exhibited reduced maternal blood-volume fraction, as well as reduced area of circulatory bed and fetal growth retardation [18,35,36]. *Akt1*$^{+/-}$ female mice were mated with *Akt1*$^{+/-}$ males (n = 17 dams, 128 fetuses/placentas), to generate fetuses of

different genetic backgrounds within the same pregnancy (*Akt1*$^{+/+}$: 38 fetuses, *Akt1*$^{+/-}$: 63 fetuses, *Akt1*$^{-/-}$: 27 fetuses). All pregnant mice were analyzed by sequential imaging modalities, as described above. Fetal implantation location was found to be randomly distributed along the uterine horn for all genotypes ($P=0.8941$). Placental peak BD-ASL values positively correlated with the relative location of fetuses along the uterine horn (r = 0.63, $P<0.0001$; Fig. S2). Consistent with the previously reported hypovascularity of Akt1$^{-/-}$ placenta, placental |BD-ASL| and PBVm values (Fig. 6A and 6B) were significantly lower ($P<0.02$) for *Akt1*$^{-/-}$ placentas (|BD-ASL| = 3.2 ± 0.6; PBVm: 0.045 ± 0.006 ml) and *Akt1*$^{+/-}$ placentas (|BD-ASL| = 3.2 ± 0.3; PBVm: 0.051 ± 0.003 ml), compared to *Akt1*$^{+/+}$ placentas (|BD-ASL| = 4.7 ± 0.4; PBVm: 0.067 ± 0.004 ml).

We next evaluated the possible influence of *Akt1*$^{-/-}$ placentas on their adjacent *Akt1*$^{+/+}$ neighbors, and interestingly, found elevated PBVm values for *Akt1*$^{+/+}$ placentas that were positioned near *Akt1*$^{-/-}$ placentas (one or two) as compared to *Akt1*$^{+/+}$ placentas that were not near *Akt1*$^{-/-}$ placentas (Fig. 6D; 1257 ± 141 vs. 792 ± 71, respectively; $P=0.0177$). |BD-ASL| values showed a similar trend (Fig. 6C; 5.8 ± 0.6 vs. 4.5 ± 0.5, respectively; $P=0.0712$). Thus, healthy fetuses benefitted from having an *Akt1*-deficient near-neighbor sibling, in contradistinction to the detrimental neighbor effect of spontaneous pathologies.
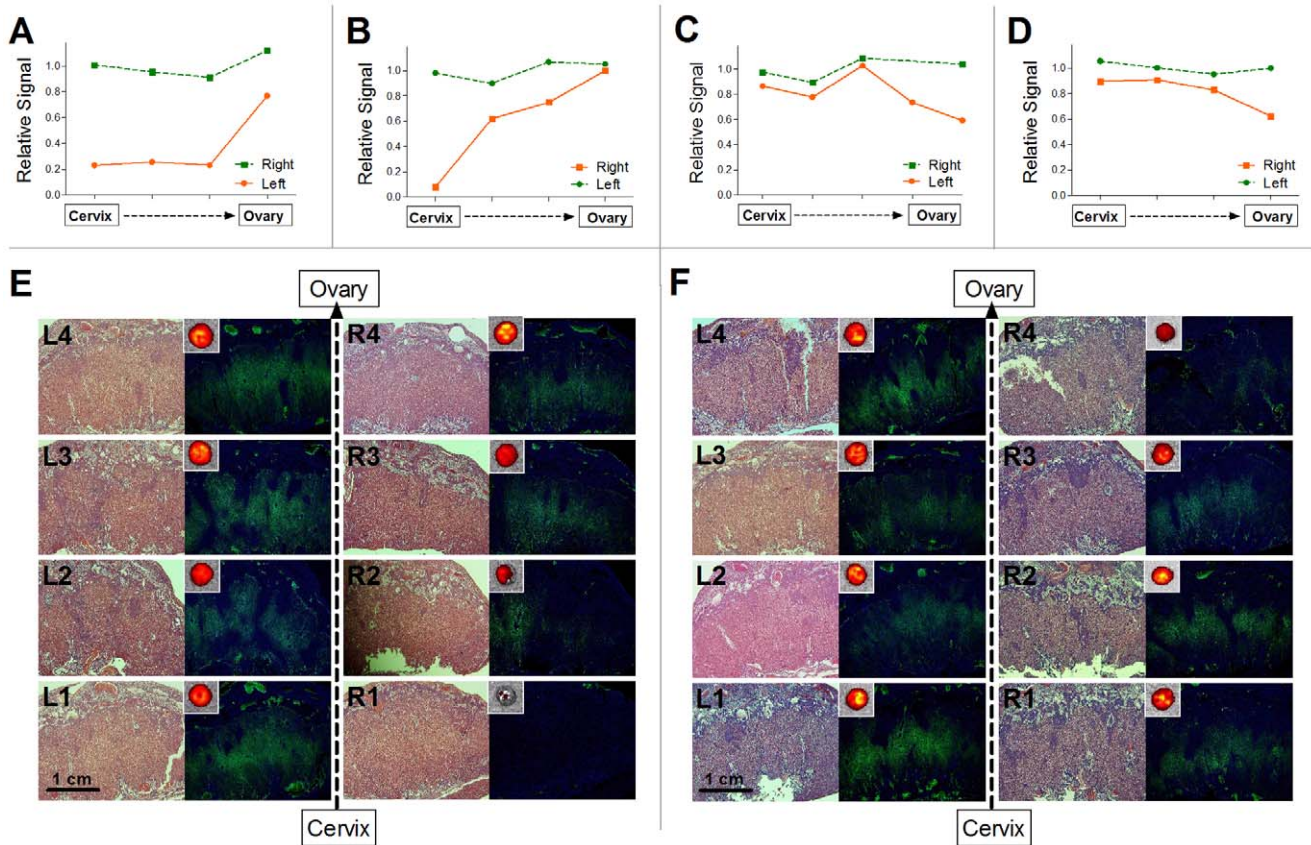
Figure 3. Contribution of arterial blood supply to the placenta. Arterial ligations were performed on ICR pregnant mice (E17.5) for either the uterine branch of the ovarian artery (n = 10 mice, 5 mice on each side; 82 placentas/fetuses); or in the uterine artery (n = 10 mice, 5 mice on each side; 92 placentas/fetuses). (A, B) Relative fluorescence signal in placentas along two uterine horns upon ligation of the left (A) or the right (B) uterine artery (each graph presents data from one animal. orange: ligated uterine horn; green: non-ligated uterine horn). (C, D) Relative fluorescence signal in placentas along two uterine horns upon ligation of the left (C) or right (D) ovarian artery (each graph presents data from one animal). (E, F) Histological sections of the placentas along two uterine horns upon ligation of the right uterine artery (E; same animal as in panel B) or right ovarian artery (F; same animal as in panel (D) Left) H&E section. Right) fluorescence microscopy (right; Green = FITC-dextran; Blue = DAPI; inset fluorescent image of the ex vivo placenta).

doi:10.1371/journal.pone.0052273.g003

Simulating Placental Function in the Mouse Pregnancy as an Electrical Circuit Reveals a Possible Hemodynamic Basis for the Observed 'Position Dependence' and 'Neighbor Effects'

Based on the experimental data reported here, we suggest a modified scheme for the functional anatomy of the mouse uterus, with its dual arterial blood supply, in late gestation (Fig. 7A, 7B). Specifically, each of the placentas can be nourished by branches from both arterial blood supplies (i.e., uterine artery and uterine branch of the ovarian artery), but in different proportions, depending on their positions along the uterine horn. The hemodynamics of such a vascular system was modeled by an electrical circuit (Fig. 7C, 7D).

The maternal heart was modeled as a battery (V_H). Blood flow in each of two uterine horns was modeled by the respective currents: $I_{ua(l/r)}$ for the left or right uterine arteries and $I_{oa(l/r)}$ for the left or right uterine branch of the ovarian artery. The balance between $I_{ua(l/r)}$ and $I_{oa(l/r)}$ was set as 3:1 using resistors near the battery. Resistance to flow along the uterine branch of the ovarian artery and the uterine artery was modeled by a series of identical resistors (one per implantation site). Resistance to flow into the placenta via the spiral arteries was modeled by low-value, flow-limiting resistors. These resistors were connected separately to a second resistor to ground, simulating exchange within the placenta itself and subsequent flow back to ground (i.e., clearance of blood through the maternal veins). Diffusion across the placenta was modeled by the insertion of a large resistor (20× the value of the dual resistors to ground representing flow into the placenta), between the dual arterial-input resistors. Total maternal blood supply to each placenta $I_{p,i}$ was therefore equal to $I_{p,oa,i}+I_{p,ua,i}$.

We used the electrical model to simulate maternal perfusion in a normal multi-fetal pregnancy (e.g., five fetuses in each uterine horn; Fig. 8A). These simulations reproduced the reduced perfusion of the central fetal positions. Interestingly, when we simulated a hypothetical case in which the resistance along the uterine and ovarian arteries was very low, this U-shaped pattern flattened, resulting in identical Ip values for all placentas.

Next, we simulated the impact of cardiac adaptation by altering the output voltage of the battery. For a fixed battery voltage, V_H, simulating a larger litter size resulted in decreased I_p for all positions, and particularly for the central positions (Fig. 8B). However, maternal cardiac output can adapt to support the growing fetuses [4–6]. To model this phenomenon, separate simulations were performed, in which V_H was adjusted to maintain the same average I_p as in the case of five fetuses per uterine horn. A 40% increase in V_H was required to match the
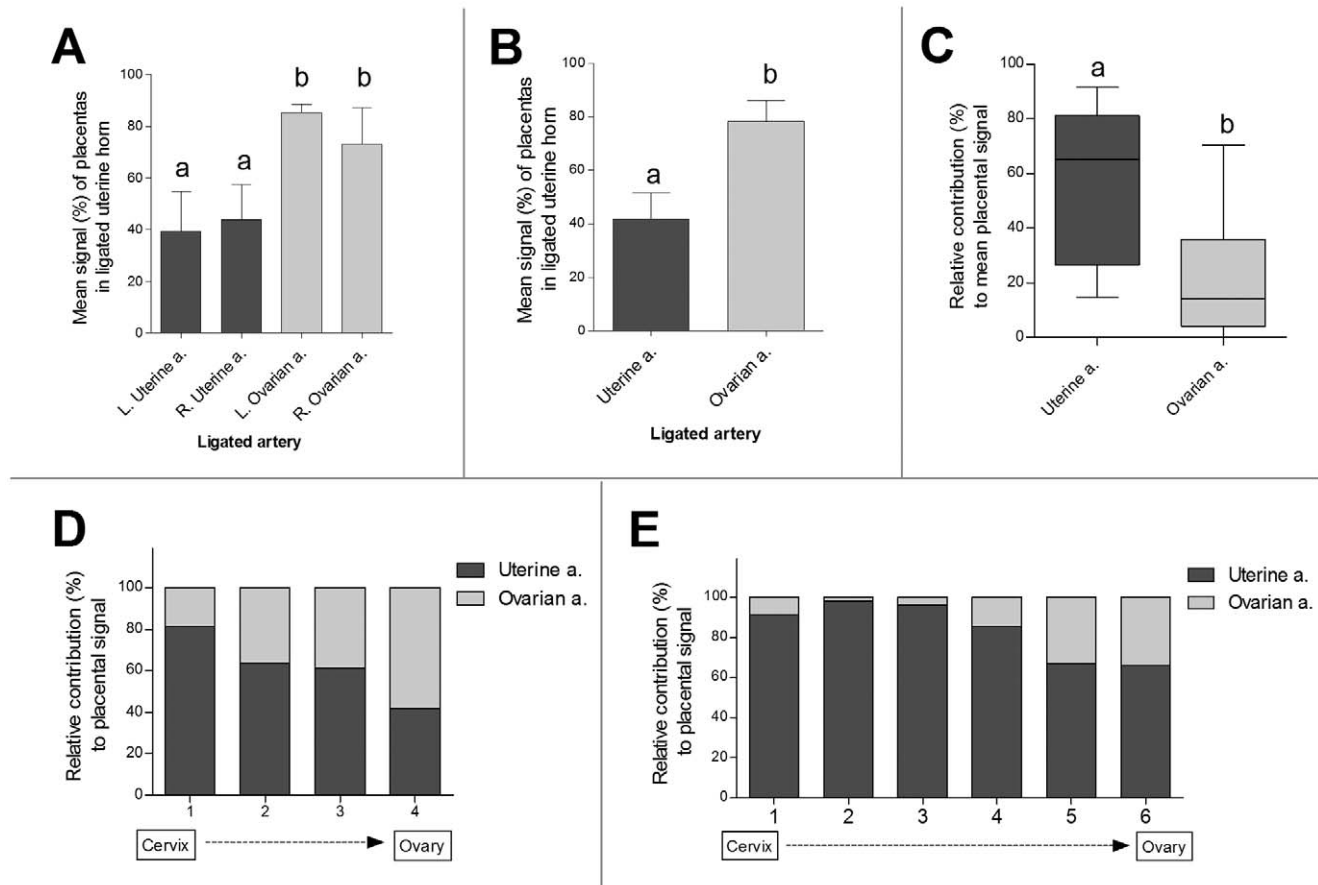
Figure 4. Arterial delivery of maternal blood to the placentas is dependent on litter size and on the position of the placenta along the uterine horn. (A) Mean fluorescence signal in placentas of a uterine horn after ligation of the left uterine a. (artery), right uterine a., left ovarian a., or right ovarian a. (n = 5 animal/group). For each animal, values were normalized (%) to the mean fluorescence signal of the placentas in the contralateral, non-ligated horn (mean ± SEM; a,b significant differences: $P < 0.05$). (B) Mean fluorescence signal in placentas of a uterine horn after unilateral ligation of the uterine or ovarian arteries (n = 10 animal/group, left and right sides combined). For each animal, values were normalized (%) to the mean fluorescence signal of the placentas in the contralateral non-ligated horn (mean ± SEM; a,b significant differences: $P < 0.05$). (C) Overall relative contributions of the uterine and ovarian arteries to the mean fluorescence signal in placentas in a uterine horn. Data are presented as Box-and-whisker plots, with the median, the 25% and 75% percentile ranges (box depth), and the maximum and minimum (T-bars). Significant differences (a, b; $P < 0.05$). (D) Relative contributions of the uterine and ovarian arteries to the fluorescence signal in placentas located in different positions along the horn. Data were extracted only from symmetric pregnancies that contained 4 fetuses in each horn (n = 5 dams). (E) Relative contributions of the uterine and ovarian arteries to the fluorescence signal in placentas located in different positions along the horn. Data were extracted only from symmetric pregnancies that contained 6 fetuses in each horn (n = 4 dams).
doi:10.1371/journal.pone.0052273.g004

average I_p for a litter of 9 fetuses to that of a litter of 5 fetuses (Fig. 8C).

Electrical modeling of the impact of arterial ligations. Simulating ligation of either of the two main arteries (i.e., setting either I_{ua} or I_{oa} to zero), resulted in reduced I_p for all positions (Fig. 8). The effect on I_p of setting $I_{ua} = 0$ (simulating ligation of the uterine artery) was larger than setting $I_{oa} = 0$. The largest impact was for lower positions for $I_{ua} = 0$ and upper positions for $I_{oa} = 0$ (Fig. 8C, 8D). The pattern in this simulation reproduced the experimental results, with I_p increasing gradually in placentas further away from the ligation point.

Simulating the 'neighbor effects' of genetic or spontaneous pathologies. To simulate the placenta of a fetus that spontaneously died during mid pregnancy, we increased the resistance of the two arterial inputs by a factor of two, while decreasing the resistance to ground by a factor of 10. The rationale for these changes was that in a dead fetus, with little or no maternal-to-placenta exchange, the resistance to flow within the

placenta should decrease, while the resistance of the arterial inputs to the placenta should increase, reflecting the expected higher restriction of flow into the placenta. The current flowing in normal 'placentas' located closest to the dead fetus was reduced (Fig. 8F), consistent with in vivo BD-ASL MRI and fluorescence experiments.

Finally, we examined the effect of a dead fetus in a model system of pregnancy having only one arterial supply (either the uterine artery or the uterine branch of the ovarian artery). Following the death of a fetus, simulated by altering its resistance as described above, I_p decreased for all positions (data not shown). By contrast, for a dual arterial supply, the 'placentas' that suffered the largest percentage decrease in current were the nearest neighbors, with less remarkable changes in the rest of the 'placentas' in that uterine horn.

It was previously reported that $Akt1^{-/-}$ placentas have a two-fold lower maternal blood volume fraction and a reduced placental circulatory bed (i.e., placental labyrinth, including both
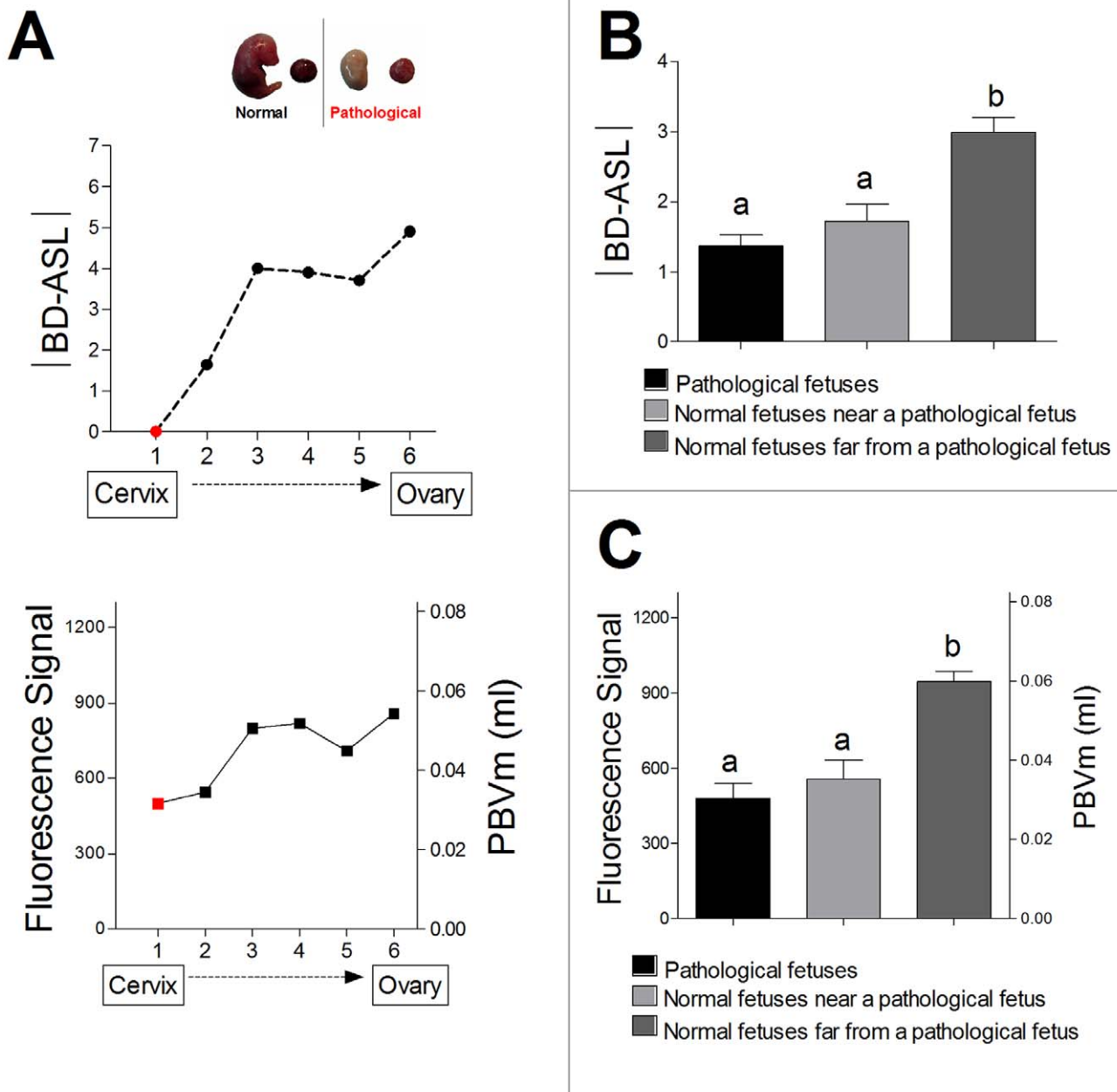
Figure 5. Intra-uterine neighbor effect: reduced |BD-ASL| and PBVm in placenta positioned adjacent to a pathological/dead fetus.
(A) A representative example from one animal; placental |BD-ASL| (upper panel), and placental fluorescence signal with the corresponding PBVm values (lower panel) of placentas along a uterine horn that contains one pathological fetus (#1, marked in red). The upper image presents the pathological fetus and its placenta adjacent to a normal fetus and placenta (fetus #3). Note the reductions in |BD-ASL| and PBVm values in the placenta of the pathological fetus, as well as in the adjacent placenta (#2). (B) Mean |BD-ASL| values in placentas of pathological/dead fetuses, fetuses positioned adjacent to pathological/dead fetus, and normal fetuses located far from a pathological/dead fetus. Note that mean |BD-ASL| value is significantly lower for those fetuses that have a pathological/dead neighbor. Different letters above bars indicate significant differences (mean ± SEM; a,b, $P < 0.05$) (C) Fluorescence values and corresponding PBVm values in placentas of pathological/dead fetuses, fetuses located near a pathological/dead fetus, and normal fetuses located distant from a pathological/dead fetus. Note that mean fluorescence value and PBVm values are significantly lower for those fetuses that have a pathological/dead neighbor (mean ± SEM; a,b, $P < 0.05$).
doi:10.1371/journal.pone.0052273.g005

maternal and fetal blood spaces) [18,35]. Accordingly, using the electrical model, an $Akt1^{-/-}$ placenta was simulated by two-fold higher resistance. As expected, $I_{p,Akt1-/-}$ was lower than that of $Akt1^{+/+}$. Remarkably, the average $I_{p,Akt1+/+}$ with an $Akt1^{-/-}$ neighbor was found to be 5% higher than that of $Akt1^{+/+}$ placentas having only $Akt1^{+/+}$ neighbors (Fig. 8G).

Discussion

During the course of pregnancy, coordinated growth and remodeling of the maternal vasculature, as well as adaptation in the maternal cardiovascular system, are essential for meeting the requirements of the growing fetus(es), and responding to challenges of physiologic and/or pathologic conditions. In litter-
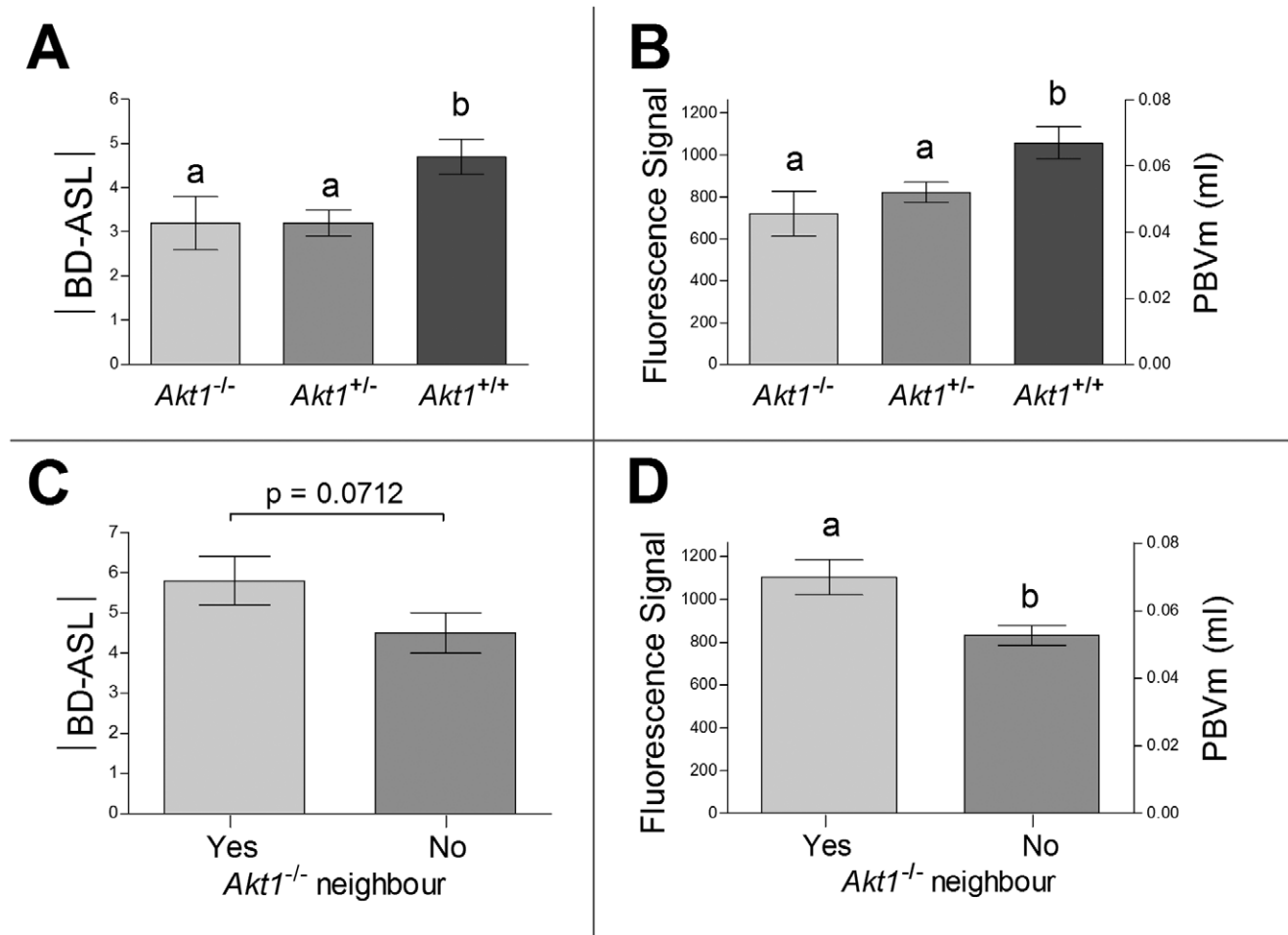
Figure 6. Placenta of *Akt1*$^{+/+}$ positioned adjacent to an *Akt1*$^{-/-}$ placenta/fetus showed increased |BD-ASL| and PBVm. (A) |BD-ASL| values in placentas of fetuses of different *Akt1* genotypes (mean ± SEM; a, b, $P<0.05$). (B) Fluorescence values and PBVm values in placentas of fetuses of different *Akt1* genotypes (mean ± SEM; a, b, $P<0.05$). (C) |BD-ASL| values in *Akt1*$^{+/+}$ placentas located near an *Akt1*$^{-/-}$ fetus, as compared to *Akt1*$^{+/+}$ placentas not located near an *Akt1*$^{-/-}$ fetus (mean ± SEM; $P=0.0712$). (D) Fluorescence values and PBVm values in *Akt1*$^{+/+}$ placentas located near a *Akt1*$^{-/-}$ fetus, as compared to *Akt1*$^{+/+}$ placentas not located near an *Akt1*$^{-/-}$ fetus (mean ± SEM; a, b, $P<0.05$).
doi:10.1371/journal.pone.0052273.g006

bearing mammals, these qualities are particularly important, as these species must support multiple fetuses within one uterus. The unique functional hemodynamic basis of the maternal vasculature system and the related in utero positional- and inter-fetal dependent effects are the focus of this study.

Using a multimodal, longitudinal imaging strategy, which included BD-ASL MRI, intra-vital microscopy, and fluorescence imaging, we were able to characterize the functional anatomy of the mouse pregnancy and the patterns of maternal-to-fetal water exchange, as well as the maternal blood volume, in placentas during normal pregnancy and pregnancies complicated by spontaneous, surgical and genetic interventions. Hemodynamics of the maternal blood flow was simulated numerically using an electrical model, which was structured based on the physiological findings. This model helps to explain the underlying hemodynamic basis for the observed arterial blood supply to the uterus and placentas in multi-fetal pregnancy, and allows us to explore extreme conditions that may not be accessible experimentally.

Previous studies reported that pregnancy in rodents is supported by bi-directional flow of blood within a uterine arterial loop [15,16]. This anatomical description is inconsistent with the data

reported here. We show herein that in the mouse, each placenta is supplied in parallel by dual arterial inflow originating from both of the main arteries, the uterine artery and the uterine branch of the ovarian artery, resulting in mosaic irrigation fields within each placenta. Thus, in the time frame of T_1 relaxation of water (i.e., seconds), the two arterial inputs do not mix prior to their entry into the placenta. Although we do not exclude the presence or functionality of uterine arterial anastomosis, we provide here direct experimental evidence that such anastomosis cannot be the primary mechanism for maternal arterial input to the placenta in mouse pregnancy.

The ratio of the blood supplied by the two feeding arteries varied with litter size within the uterine horn. Our results indicate that as the number of fetuses/placentas increased from 4 to 6 per uterine horn, the relative contribution of the uterine artery increased. Therefore, it appears that large-scale vascular remodeling can occur in order to meet the demands of individual pregnancies. In woman, the uterus is mainly supplied with blood by the uterine arteries, while the contribution of the ovarian arteries is less significant [41]. Interestingly, pregnancy can be established in women treated for postpartum hemorrhage and uterine myomas by either uterine artery embolization or arterial
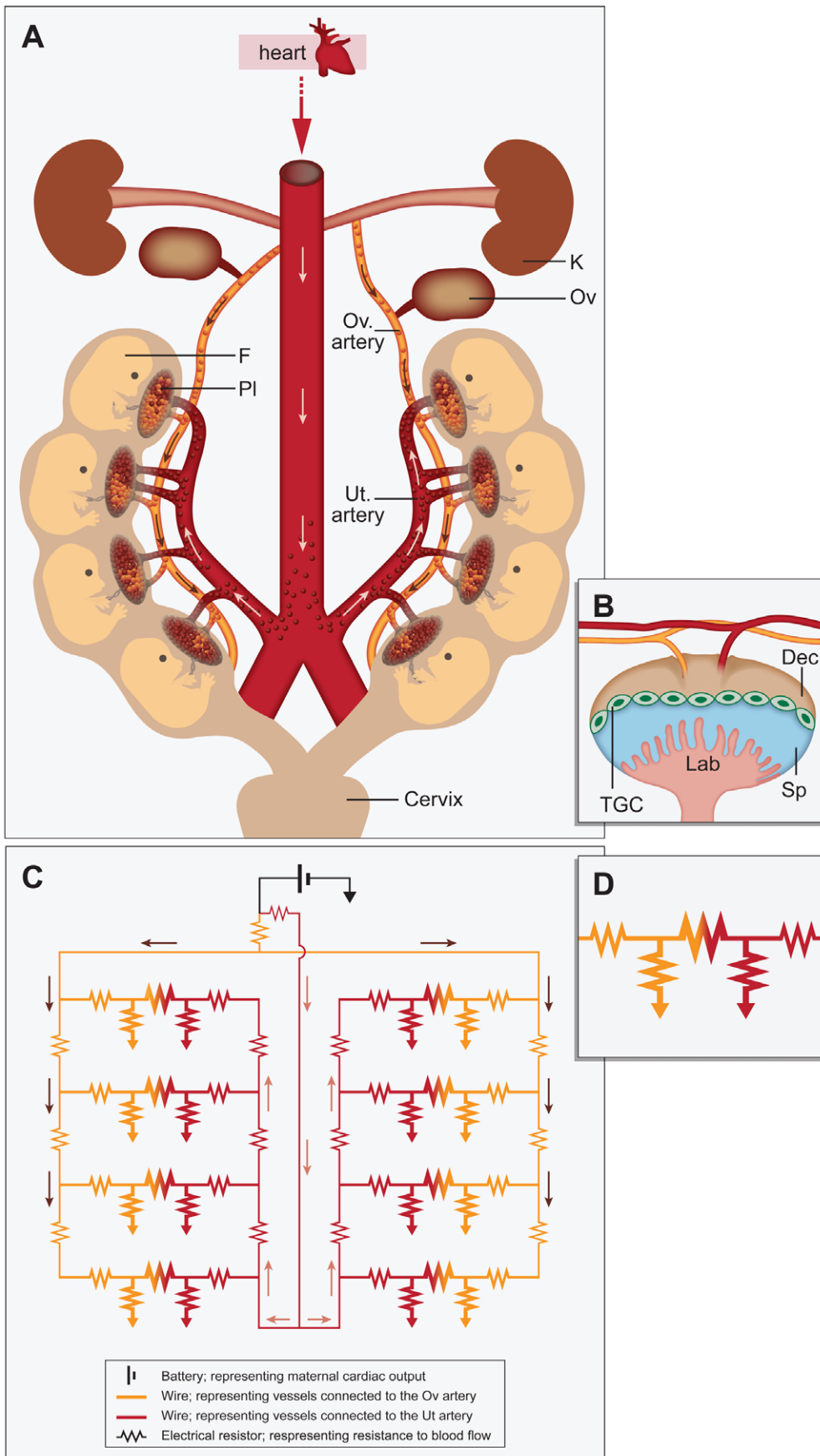
Figure 7. Electrical circuit modeling of the hemodynamics of maternal arterial supply in the mouse pregnancy. (A) Diagram of mouse uterine horns and their arterial blood vessels in the gestation period after placentas have formed (E10.5 to term). Our results demonstrate that each placenta can be perfused from two maternal arteries. F Fetus, K Kidney, Ov Ovary, Pl Placenta, Ut Uterine. (B) Schematic diagram of mouse placenta. Dec Decidua, Sp Spongiothrophoblast, TGC Throphoblast Giant Cells, Lab Labyrinth. (C) Numerical simulation of blood flow in multi-fetus pregnancy modeled as an electrical circuit. Bi-directional blood flow in each of two uterine horns was modeled by the respective currents: $I_{ua(l/r)}$ for the left or right uterine arteries and $I_{oa(l/r)}$ for the left or right uterine branch of the ovarian artery. The balance between $I_{ua(l/r)}$ and $I_{oa(l/r)}$ was set at 3:1 using resistors placed into the circuit near the battery. Resistance to flow along the uterine branch of the ovarian artery and the uterine artery was modeled by a series of identical resistors (one per implantation site). (D) Placenta modeled as an electrical circuit. Resistance to flow into the placenta via the spiral arteries was modeled by low-value resistors, which were connected separately to a second resistor to ground, simulating exchange within the placenta itself and the flow back to ground (i.e., clearance of blood through the maternal veins). Diffusion across the placenta was modeled by the insertion of a large resistor (20× the value of the dual resistors to ground representing flow into the placenta), between the dual arterial input resistors. Total maternal blood supply to each placenta $I_{p,i}$ was therefore derived from $I_{p,oa,i}+I_{p,ua,i}$. Arrows indicate the direction of flow.
doi:10.1371/journal.pone.0052273.g007

ligation, providing a human example of this remodeling of collateral blood flow [42].

As expected, an increased number of fetuses per uterine horn was associated with reduced fetal body weight. Such systemic effects could be attributed to a drop in maternal blood pressure associated with the increased fetal load, competition among fetuses for a limited amount of space, as well as gas and nutrient transport insufficiency [43]. One mechanism of compensating for the reduced placenta inflow in large litters is an increase in cardiac output during pregnancy, as was shown previously in many species [4–6,44].

A dual arterial supply to each placenta provides robustness to the maternal support of pregnancy. As mentioned above, fetuses located at the edges of the uterine horn appear to enjoy more favorable growth conditions vis-à-vis blood flow and volume. However, according to our data, we speculate that those fetuses located in the middle of the uterine horn may be less susceptible to damage when one of the maternal arteries is compromised. Therefore, the dual arterial design of the placenta may confer a growth advantage to the fetuses at both edges of the horn in unperturbed pregnancy, while providing a survival advantage to fetuses located in the middle of the uterine horn in cases of severe maternal arterial damage.

The complex design of the maternal circulation can result in interesting hemodynamic effects on fetal development. In particular, we report here that beyond the direct effect on the affected placenta, fetal-specific pathological processes, such as spontaneous fetal growth retardation or death, or even a genetic difference, occurring in an adjacent placenta, can significantly alter maternal blood inflow in the placenta of an otherwise healthy fetus. Such an effect should be added to previously reported molecular mechanisms (e.g., the local diffusion of hormones affecting gender-related changes) describing the influence of a fetus on adjacent siblings [45–47].

Interestingly, we found that the placentas of fetuses that were located closest to the pathological fetus also exhibited significantly lower maternal-to-placental exchange and maternal blood volume, compared with that expected based upon their position along the uterine horn. Electrical simulation of a pathological/dead fetus in a pregnancy supported by a single arterial supply (either the uterine artery or the ovarian artery) resulted in a significant decrease in the current flowing in all of the placentas located downstream of the pathological/dead one, with a small systemic effect in placentas located upstream of it. Such simulations highlighted the robustness of the dual arterial blood supply to the uterine horn, which is able to compensate for the loss of a single fetus and sustain blood flow to the remaining siblings.

To evaluate the effects of genetic heterogeneity within a single litter on possible in utero environmental factors, an Akt1 model was employed. $Akt1^{+/-}$ female mice were mated with $Akt1^{+/-}$ males in order to generate fetuses of all possible genetic

backgrounds within the same pregnancy, with the same maternal genetic background. This allowed us to investigate inter-fetal effects without confounding effects related to maternal genotype. $Akt1^{-/-}$ placentas were reported previously to have reduced vasculature and smaller areas of exchange within the labyrinth [18,35]. Furthermore, the $Akt1^{-/-}$ fetuses were shown to be small, with defective vasculature, suggesting $Akt1^{-/-}$ as a genetic model for human IUGR. Consistent with these studies, we demonstrated that $Akt1^{-/-}$ placentas showed reduced maternal-to-placental exchange and maternal blood volume compared to $Akt1^{+/+}$ placentas. Interestingly, we found that $Akt1^{+/+}$ placentas positioned adjacent to $Akt1^{-/-}$ placentas displayed a significant increase in both their BD-ASL MRI values and ex vivo fluorescence signals compared to $Akt1^{+/+}$ placentas situated near other normal placentas. This finding suggests that the presence of a small, IUGR-like fetus with placental insufficiency might actually improve placental perfusion in its wild-type neighbouring siblings. In accordance, the hemodynamic effects of $Akt1^{-/-}$ placentas on the neighboring placenta could be simulated using the electrical model by increasing their resistance by a factor of 2. Furthermore, since metabolism and nutrient demand of $Akt1^{-/-}$ fetuses may be reduced, it is reasonable to speculate that adjacent $Akt1^{+/+}$ fetuses would benefit, adding a potential metabolic component to the complexity of the reported MR hemodynamic measurements.

The hemodynamic effects of genetic or spontaneous pathologies show that in addition to the systemic effects, which impact the litter as whole, maternal arterial supply might be different for different fetuses in the uterus, such that maternal supply to one placenta can be directly affected by the condition of the neighboring placentas. Moreover, these findings provide an example of how fetal growth must be accommodated by corresponding adaptation of the maternal vasculature. An important implication of this finding is that variability of phenotypes in genetic mouse models could arise from the location and order of fetuses of different genotypes along the uterine horn. As a consequence, in future studies that examine phenotypes of fetuses/pups of different genotypes, confounding local and environmental in utero effects should be considered, both for each individual fetus, and in combination with the genotype of its adjacent siblings. Furthermore, since Akt was found to play a critical role in angiogenesis, cell survival and differentiation, and metabolism, future studies should further elucidate the possible effects of the mother genotype on placental development and function in combination with the in utero environment.

In summary, the current study demonstrated the unique functional architecture of the dual arterial supply, which supports robust maternal circulation in the mouse pregnancy, thus sustaining large-litter pregnancies. The experiments revealed complex intra-uterine environmental interactions that exert a significant impact on fetal development and placental function. In particular, we discovered distinctive hemodynamic effects of fetal
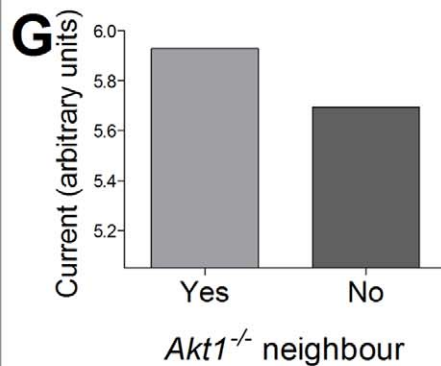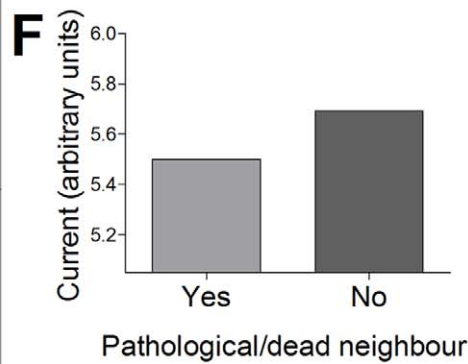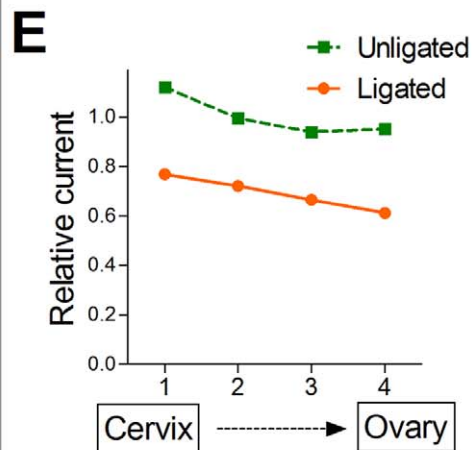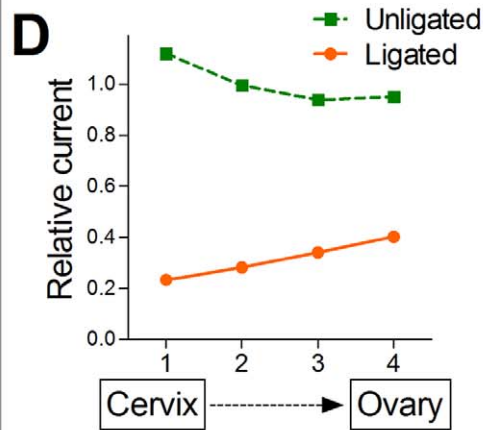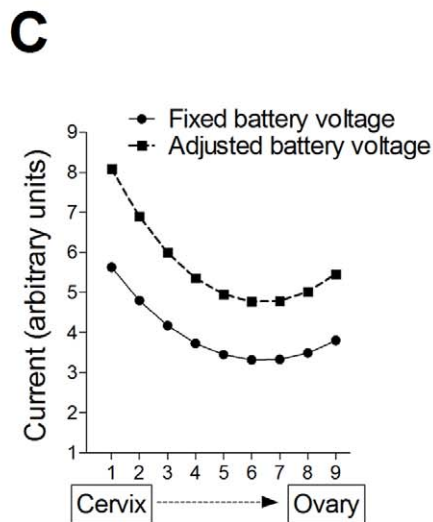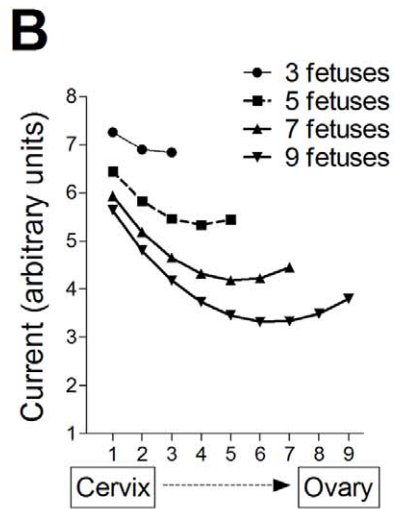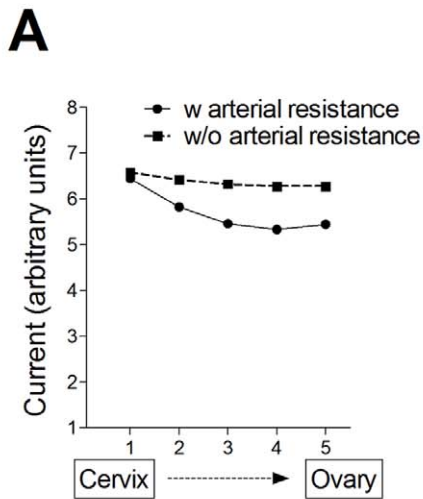
Figure 8. Numerical simulation of placental function in the pregnant mouse reveals a possible hemodynamic basis for the observed 'position dependence' and 'neighbor effects'. (A) Simulation performed for the case of five fetuses in a single uterine horn and a hypothetical case, in which the resistance along the uterine and ovarian arteries was very low. Note the flattening of the U-shaped pattern in the latter case. (B) Simulation of the effect of increasing litter size with a fixed battery voltage V_H (no cardiac output compensation). (C) Simulating a case of nine 'fetuses/placentas' with adjustment of V_H (i.e., adjustment of cardiac output) to maintain the same average I_p as in the case of five fetuses per uterine horn. (D) Ligation simulations of the uterine artery showing I_p of placentas in the non-ligated and ligated horns, normalized to the average I_p of the non-ligated horn. (E) Ligation simulations of the uterine branch of the ovarian artery showing I_p of placentas in the non-ligated and ligated horns, normalized to the average I_p of the non-ligated horn. (F) Simulation of the placenta of a fetus that spontaneously died during mid pregnancy. The current flowing in normal placentas located closest to the dead fetus is compared to placentas located distant from the dead fetus. The dead fetus was simulated by reduced placental resistance compared to normal placentas. (G) Simulation of $Akt1^{-/-}$ placenta; the average $I_{p,Akt1+/+}$ of $Akt1^{+/+}$ having a $Akt1^{-/-}$ neighbor compared with $Akt1^{+/+}$ placentas having only $Akt1^{+/+}$ neighbors. The $Akt1^{-/-}$ placenta was simulated as increased resistance compared to $Akt1^{+/+}$ placentas.
doi:10.1371/journal.pone.0052273.g008

position on placental perfusion, and hemodynamic effects of genetic or spontaneous pathologies on adjacent neighbouring siblings. The presence of the genetically defective placenta of an $Akt1^{-/-}$ fetus was associated with increased maternal-to-fetal exchange and increased maternal blood volume in the placenta of its nearest $Akt1^{+/+}$ siblings. Conversely, the presence of a spontaneously pathological/dead fetus in utero was associated with significantly reduced maternal-to-fetal exchange and reduced maternal blood volume in the placenta of its nearest siblings. These findings highlight the complexity of prenatal development in litter-bearing mammals. Remarkably, the dual arterial supply is also conserved in mammals bearing a single offspring, including primates [48].

Supporting Information

Figure S1 Calibration between ex vivo fluorescence signal and the placental maternal blood volume (PBVm). To correlate the normalized placental fluorescence signal with the placental maternal blood volume (PBVm), a calibration experiment was performed. Dextran-FITC was intravenously injected into female ICR mice at E17.5 (n = 6), and blood samples were drawn from each mouse 10 min later. The fluorescence signals of fixed blood volumes (0.01, 0.03, 0.05, 0.08, 0.1, 0.15 and 0.3 ml) were measured, and were normalized, in each mouse, to the signal in the uterine artery. Ex vivo fluorescence signal intensities were positively correlated to blood volume (r = 0.97, $P<0.0001$), thereby establishing a calibration equation for calculating placental maternal blood volume from normalized fluorescence signal: $PBVm\ (ml) = \left[6.34e^{-5} \times (normalized\ fluorescence\ signal)\right] - 1.2e^{-4}$
(TIF)

Figure S2 Correlation between peak BD-ASL values and the relative location of fetuses along the uterine horn in $PKBAkt1^{-/-}$ pregnant mice (E17.5) carry fetuses of different genotype. Peak BD-ASL values showed significant

positive correlation with the position of placentas along the uterine horn (r = 0.63, $P<0.0001$). Note that fetal implantation location was randomly distributed along the uterine horn for all genotypes ($P = 0.8941$).
(TIF)

Movie S1 Intravital microscopy of surgically-exposed intact uterine horn following intravenous administration of fluorescent FITC-dextran.
(MPG)

Movie S2 Intravital microscopy of surgically-exposed uterine horn following ligation of the uterine artery and intravenous administration of fluorescent FITC-dextran.
(MPG)

Movie S3 Intravital microscopy of surgically-exposed uterine horn following ligation of the uterine branch of the ovarian artery and intravenous administration of fluorescent FITC-dextran.
(MPG)

Author Contributions

Conceived and designed the experiments: MN JRG TR RA. Performed the experiments: TR RA YA YC. Analyzed the data: TR RA JRG MN. Contributed reagents/materials/analysis tools: BH AJJ. Wrote the paper: TR RA MN JRG.

References

1. Poppas A, Shroff SG, Korcarz CE, Hibbard JU, Berger DS, et al. (1997) Serial assessment of the cardiovascular system in normal pregnancy. Role of arterial compliance and pulsatile arterial load. Circulation 95: 2407–2415.
2. Khankin EV, Royle C, Karumanchi SA (2010) Placental Vasculature in Health and Disease. Semin Thromb Hemost 36: 309–320.
3. Osol G, Mandala M (2009) Maternal uterine vascular remodeling during pregnancy. Physiology (Bethesda) 24: 58–71.
4. Kulandavelu S, Qu D, Adamson SL (2006) Cardiovascular function in mice during normal pregnancy and in the absence of endothelial NO synthase. Hypertension 47: 1175–1182.
5. Eghbali M, Deva R, Alioua A, Minosyan TY, Ruan H, et al. (2005) Molecular and functional signature of heart hypertrophy during pregnancy. Circ Res 96: 1208–1216.
6. Wong AY, Kulandavelu S, Whiteley KJ, Qu D, Langille BL, et al. (2002) Maternal cardiovascular changes during pregnancy and postpartum in mice. Am J Physiol Heart Circ Physiol 282: H918–925.
7. McGrath CJ (1984) Anesthesia for cesarean section in large animals. Mod Vet Pract 65: 522–524.
8. Valdes G, Corthorn J (2011) Challenges posed to the maternal circulation by pregnancy. Integr Blood Press Control 4: 45–53.
9. Jayet PY, Rimoldi SF, Stuber T, Salmon CS, Hutter D, et al. (2010) Pulmonary and systemic vascular dysfunction in young offspring of mothers with preeclampsia. Circulation 122: 488–494.
10. Barker DJ (1999) Fetal origins of cardiovascular disease. Ann Med 31 Suppl 1: 3–6.
11. Groenenberg IA, Wladimiroff JW, Hop WC (1989) Fetal cardiac and peripheral arterial flow velocity waveforms in intrauterine growth retardation. Circulation 80: 1711–1717.
12. Noori M, Donald AE, Angelakopoulou A, Hingorani AD, Williams DJ (2010) Prospective study of placental angiogenic factors and maternal vascular function before and after preeclampsia and gestational hypertension. Circulation 122: 478–487.
13. Barker DJ, Gluckman PD, Godfrey KM, Harding JE, Owens JA, et al. (1993) Fetal nutrition and cardiovascular disease in adult life. Lancet 341: 938–941.
14. Barker DJ, Winter PD, Osmond C, Margetts B, Simmonds SJ (1989) Weight in infancy and death from ischaemic heart disease. Lancet 2: 577–580.

15. Ginther OJ (1974) Internal regulation of physiological processes through local venoarterial pathways: a review. J Anim Sci 39: 550–564.
16. Vom Saal FS, Dhar MG (1992) Blood flow in the uterine loop artery and loop vein is bidirectional in the mouse: implications for transport of steroids between fetuses. Physiol Behav 52: 163–171.
17. McLaren A, Michie D (1960) Control of Pre-natal growth in mammals. Nature 187: 3.
18. Plaks V, Berkovitz E, Vandoorne K, Berkutzki T, Damari GM, et al. (2011) Survival and size are differentially regulated by placental and fetal PKBalpha/AKT1 in mice. Biol Reprod 84: 537–545.
19. Plaks V, Sapoznik S, Berkovitz E, Haffner-Krausz R, Dekel N, et al. (2011) Functional phenotyping of the maternal albumin turnover in the mouse placenta by dynamic contrast-enhanced MRI. Mol Imaging Biol 13: 481–492.
20. Walls JR, Coultas L, Rossant J, Henkelman RM (2008) Three-dimensional analysis of vascular development in the mouse embryo. PLoS One 3: e2853.
21. Girsh E, Plaks V, Gilad AA, Nevo N, Schechtman E, et al. (2007) Cloprostenol, a prostaglandin F(2alpha) analog, induces hypoxia in rat placenta: BOLD contrast MRI. NMR Biomed 20: 28–39.
22. Nieman BJ, Turnbull DH (2010) Ultrasound and magnetic resonance microimaging of mouse development. Methods Enzymol 476: 379–400.
23. Plaks V, Kalchenko V, Dekel N, Neeman M (2006) MRI analysis of angiogenesis during mouse embryo implantation. Magn Reson Med 55: 1013–1022.
24. Tomlinson TM, Garbow JR, Anderson JR, Engelbach JA, Nelson DM, et al. (2010) Magnetic resonance imaging of hypoxic injury to the murine placenta. Am J Physiol Regul Integr Comp Physiol 298: R312–319.
25. Dickinson ME (2006) Multimodal imaging of mouse development: tools for the postgenomic era. Dev Dyn 235: 2386–2400.
26. Orita J, Sato E, Saburi S, Nishida T, Toyoda Y (1996) Magnetic resonance imaging of the internal structure of the mouse fetus. Exp Anim 45: 171–174.
27. Spurney CF, Lo CW, Leatherbury L (2006) Fetal mouse imaging using echocardiography: a review of current technology. Echocardiography 23: 891–899.
28. Shen Y, Leatherbury L, Rosenthal J, Yu Q, Pappas MA, et al. (2005) Cardiovascular phenotyping of fetal mice by noninvasive high-frequency ultrasound facilitates recovery of ENU-induced mutations causing congenital cardiac and extracardiac defects. Physiol Genomics 24: 23–36.
29. O'Leary-Moore SK, Parnell SE, Lipinski RJ, Sulik KK (2011) Magnetic resonance-based imaging in animal models of fetal alcohol spectrum disorder. Neuropsychol Rev 21: 167–185.
30. Tobita K, Liu X, Lo CW (2010) Imaging modalities to assess structural birth defects in mutant mouse models. Birth Defects Res C Embryo Today 90: 176–184.
31. Cohen B, Ziv K, Plaks V, Israely T, Kalchenko V, et al. (2007) MRI detection of transcriptional regulation of gene expression in transgenic mice. Nat Med 13: 498–503.
32. Salomon LJ, Siauve N, Balvay D, Cuenod CA, Vayssettes C, et al. (2005) Placental perfusion MR imaging with contrast agents in a mouse model. Radiology 235: 73–80.
33. Riesterer O, Zingg D, Hummerjohann J, Bodis S, Pruschy M (2004) Degradation of PKB/Akt protein by inhibition of the VEGF receptor/mTOR pathway in endothelial cells. Oncogene 23: 4624–4635.
34. Riley JK, Carayannopoulos MO, Wyman AH, Chi M, Ratajczak CK, et al. (2005) The PI3K/Akt pathway is present and functional in the preimplantation mouse embryo. Dev Biol 284: 377–386.
35. Yang ZZ, Tschopp O, Hemmings-Mieszczak M, Feng J, Brodbeck D, et al. (2003) Protein kinase B alpha/Akt1 regulates placental development and fetal growth. J Biol Chem 278: 32124–32131.
36. Chen WS, Xu PZ, Gottlob K, Chen ML, Sokol K, et al. (2001) Growth retardation and increased apoptosis in mice with homozygous disruption of the Akt1 gene. Genes Dev 15: 2203–2208.
37. Kent LN, Ohboshi S, Soares MJ (2012) Akt1 and insulin-like growth factor 2 (Igf2) regulate placentation and fetal/postnatal development. Int J Dev Biol 56: 255–261.
38. Yung HW, Calabrese S, Hynx D, Hemmings BA, Cetin I, et al. (2008) Evidence of placental translation inhibition and endoplasmic reticulum stress in the etiology of human intrauterine growth restriction. Am J Pathol 173: 451–462.
39. Avni R, Raz T, Biton IE, Kalchenko V, Garbow JR, et al. (2012) Unique in utero identification of fetuses in multifetal mouse pregnancies by placental bidirectional arterial spin labeling MRI. Magn Reson Med 68: 560–570.
40. DeBosch B, Treskov I, Lupu TS, Weinheimer C, Kovacs A, et al. (2006) Akt1 is required for physiological cardiac growth. Circulation 113: 2097–2104.
41. Cicinelli E, Einer-Jensen N, Galantino P, Alfonso R, Nicoletti R (2004) The vascular cast of the human uterus: from anatomy to physiology. Ann N Y Acad Sci 1034: 19–26.
42. Berkane N, Moutafoff-Borie C (2010) Impact of previous uterine artery embolization on fertility. Curr Opin Obstet Gynecol 22: 242–247.
43. Meyer KM, Koch JM, Ramadoss J, Kling PJ, Magness RR (2010) Ovine surgical model of uterine space restriction: interactive effects of uterine anomalies and multifetal gestations on fetal and placental growth. Biol Reprod 83: 799–806.
44. Magness RR, Phernetton TM, Zheng J (1998) Systemic and uterine blood flow distribution during prolonged infusion of 17beta-estradiol. Am J Physiol 275: H731–743.
45. Ryan BC, Vandenbergh JG (2002) Intrauterine position effects. Neurosci Biobehav Rev 26: 665–678.
46. Nagao T, Wada K, Kuwagata M, Nakagomi M, Watanabe C, et al. (2004) Intrauterine position and postnatal growth in Sprague-Dawley rats and ICR mice. Reprod Toxicol 18: 109–120.
47. vom Saal FS (1981) Variation in phenotype due to random intrauterine positioning of male and female fetuses in rodents. J Reprod Fertil 62: 633–650.
48. Ramsey EM, Chez RA, Doppman JL (1979) Radioangiographic measurement of the internal diameters of the uteroplacental arteries in rhesus monkeys. Am J Obstet Gynecol 135: 247–251.